Two-dimensional superconductivity in single-band correlated 2*H*-type NbO_2 layers

Takuto Soma [1,*] Kohei Yoshimatsu [1] Koji Horiba [2,3] Hiroshi Kumigashira [2,3] and Akira Ohtomo [1,3,†]

[1]*Department of Chemical Science and Engineering, Tokyo Institute of Technology, 2-12-1 Ookayama, Meguro-ku, Tokyo 152-8552, Japan*

[2]*Photon Factory, Institute of Materials Structure Science, High Energy Accelerator Research Organization (KEK), 1-1 Oho, Tsukuba 305-0801, Japan*

[3]*Materials Research Center for Element Strategy (MCES), Tokyo Institute of Technology, Yokohama 226-8503, Japan*

(Received 6 October 2021; revised 29 January 2022; accepted 18 February 2022; published 7 March 2022)

The oxide superconductor $Li_{1-x}NbO_2$ has two-dimensional (2D) NbO_2 layers consisting of edge-shared triangular prisms. This structure is a unique oxide analog to 2*H*-type transition-metal dichalcogenides (TMDs), yet its electronic properties have not received any significant attention. Using $Li_{1-x}NbO_2$ epitaxial films, we find the 2D superconductivity associated with the Berezinskii-Kosterlitz-Thouless transition and a large anisotropy of the upper critical field. The temperature-independent anisotropy strongly suggests single-band superconductivity, in contrast to TMDs. Correspondingly, the largely isolated single d_{z^2} state revealed by synchrotron-radiation photoelectron spectroscopy and density functional theory is explained in terms of strong ligand field splitting. These results indicate that superconductivity in $Li_{1-x}NbO_2$ occurs in 2D NbO_2 layers with a narrow and correlated single band, reminiscent of superconductivity in cuprates. Our study provides insight into the unconventional correlation in the Hubbard system with a 2D triangular lattice.

DOI: 10.1103/PhysRevB.105.104504

I. INTRODUCTION

While little has become known about the electronic state of $Li_{1-x}NbO_2$ ($0 \leqslant x \leqslant 0.55$) since the discovery of its superconductivity [1], two-dimensional (2D) electronic states can be inferred from its crystal structure. Li and NbO_2 layers are stacked alternately, and each NbO_2 layer consists of edge-sharing triangular prisms along the *c* axis [Fig. 1(a)]. Except for $A_{1-x}NbO_2$ (A = Li or Na), the triangular prism unit is not found in oxides because ionic bonding favors the octahedral unit as is found in $LiMO_2$ (M = V, Cr, Co, Ni, Mo, or Rh), some of which are used as electrodes in batteries [2–5]. By contrast, triangular prism coordination is most common in 2*H*-type structure transition-metal dichalcogenides (TMDs), with 2*H*-MoS_2 showing essentially the same as that of $LiNbO_2$ [Fig. 1(b)] [6–8]. It has been reported that 2*H*-MoS_2 and 2*H*-$NbSe_2$ are excellent materials exhibiting various exotic properties, including 2D superconductivity and quantum-phase transitions [8–12]. In addition, extremely clean 2D superconductivity has been recently found in bulk Ba_3Nb_5S composed of superconducting NbS_2 and blocking Ba_6NbS_8 layers [13]. Based on TMDs and their derivatives, it can be presumed that $Li_{1-x}NbO_2$ is composed of superconducting "2*H*-NbO_2" and blocking Li layers. Given their structural similarities and superconductivity, it is worth revealing the electronic state of $Li_{1-x}NbO_2$ as an ionic analog of van der Waals materials.

We have developed a method for the epitaxial growth of superconducting $Li_{1-x}NbO_2$ [14]. The superconducting films exhibit high optical transparency in the visible range, which is unprecedented for any *p*-type superconductor. Moreover, it was suggested that strong electron correlation and high transparency arise from the large effective mass of carriers and characteristic *d*-band splitting [14,15]. Despite their structural similarities, the electronic states of $Li_{1-x}NbO_2$ differ from those of TMDs because of their opaqueness and unremarkable correlation [8–10]. In addition, the isolated *d* bands are inconsistent with a number of TMDs [6–8,16]. On the other hand, correlated phases have been recently found in TMD moiré superlattices, where the isolated narrow moiré band is explained by the Hubbard models applicable to transition-metal oxides [17,18]. Furthermore, the moiré superlattices exhibit a variety of electronic phases, such as superconducting, Mott insulating, and spin-ordered phases. The TMD-based moiré superlattices are reminiscent of cuprates and are thus regarded as a new unconventional superconductor family. Apart from TMDs, superconductivity and strong correlation in the 2*H*-NbO_2 layer have attracted our attention for further elucidation of the correlated physics in a 2D ionic compound.

In this study, the 2D characteristics and electronic states of highly crystalline bulklike $Li_{1-x}NbO_2$ epitaxial films (thickness ~100 nm) were investigated [14]. We observed clear evidence of 2D carriers in magnetotransport and strong isolation of Nb 4*d* states in photoemission spectra (PES) and x-ray absorption spectra (XAS). In particular, 2*H*-NbO_2 layers exhibited large and temperature-independent anisotropy, strongly suggesting the presence of correlated electrons in a single band. Our results present not only insight into an ionic analog of van der Waals materials but also relevance to strongly correlated Hubbard systems such as layered cuprates.

II. METHODS

Superconducting $Li_{1-x}NbO_2$ films were grown using a three-step synthesis method, the details of which are described

*soma.t.ab@m.titech.ac.jp
†ohtomo.a.aa@m.titech.ac.jp

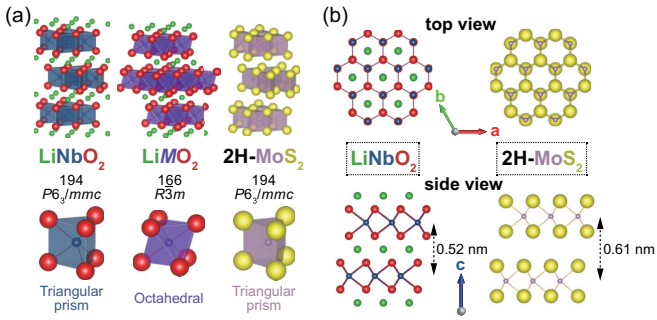

FIG. 1. (a) Schematic illustrations of each crystal with space group and structural units. (b) Crystal structures of $LiNbO_2$ and $2H$-MoS_2 projected from the c axis (top) and a axis (bottom).

in our previous report [14]. The film thickness was set to ∼100 nm, as verified using a stylus profiler. The crystal structures and epitaxial relationship were confirmed by laboratory diffraction (XRD) apparatus with Cu $K\alpha_1$ radiation (Rigaku, SmartLab). See the Supplemental Material for detailed sample properties [19]. The temperature dependence of resistivity and the magnetotransport properties were measured by a standard four-probe method using a physical property measurement system (Quantum Design, PPMS) with a rotation stage and a source meter (Keithley 2636A). The direction of the magnetic field was regulated by using a sample rotator with an accuracy of better than 0.01°.

PES and XAS measurements were performed at the BL-2A undulator beamline at the Photon Factory, KEK (Tsukuba, Japan). Samples for PES measurements were capped by several nanometers thick alumina films deposited by pulsed-laser deposition method at room temperature *in situ* to avoid surface oxidation. The PES spectra were recorded using an electron energy analyzer (SES-2002, VG Scienta) with an energy resolution of less than 150 meV at a phonon energy of 600 eV at room temperature. The E_F refers to that of the Au in electrical contact with the sample surface. XAS spectra were recorded in the total electron yield mode.

Density functional theory (DFT) calculations were performed using the QUANTUM ESPRESSO package with the details given in the Supplemental Material [19] (also see [20,21]).

III. RESULTS

A. Berezinskii-Kosterlitz-Thouless (BKT) transition

The BKT transition was investigated for a superconducting $Li_{1-x}NbO_2$ film (sample A, Supplemental Material [19]) by measuring the resistivity (ρ) in parallel with the NbO_2 layers. Figure 2 shows the current-voltage (I-V) profiles at several different temperatures near the critical temperature ($T_c = 3.5$ K). Linear I-V profiles ($V \propto I$) were obtained at T_c or temperatures above T_c. By contrast, below T_c the nonlinearity increased with decreasing temperature. The power-law dependence ($V \propto I^\alpha$, $\alpha > 1$) reflects the BKT transition, which is a characteristic of 2D systems [22]. The inset of Fig. 2 shows the exponent α (calculated as the gradient of the fitted lines) as a function of temperature. We obtained a BKT transition temperature (T_{BKT}) of 2.4 K, where $\alpha = 3$. The temperature dependence of resistivity (ρ-T) fitted the Halperin-Nelson equation [23] very well (Supplemental Material [19]). Therefore, the 2D superconducting state was verified below T_{BKT} in the $Li_{1-x}NbO_2$ films.

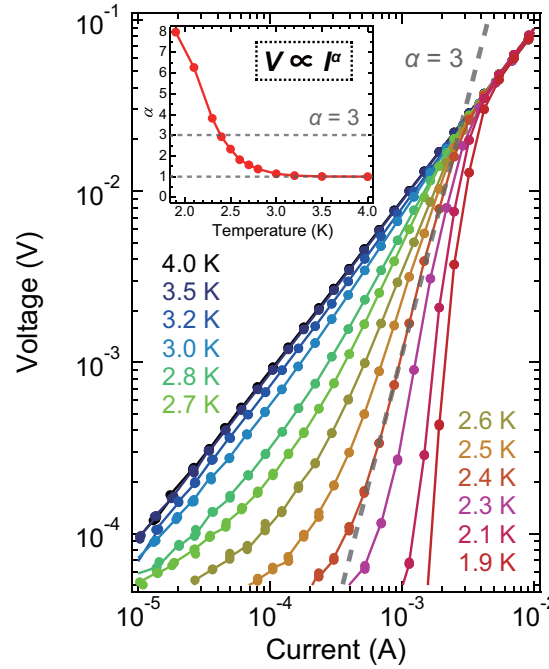

FIG. 2. Temperature dependence of I-V profiles for $Li_{1-x}NbO_2$ films (sample A). The gray broken line guides the eye for $V \propto I^3$. The inset shows the temperature dependence of the exponent α obtained by fitting I-V to $V \propto I^\alpha$. T_{BKT} is estimated as 2.4 K at the crossing point with $\alpha = 3$.

B. Large anisotropy of upper critical field

The 2D characteristics were also confirmed from the magnetotransport properties. Figures 3(a) and 3(b) show the ρ-T curves for different magnetic fields (H) for $Li_{1-x}NbO_2$ films (sample B with $T_c = 4.3$ K) measured in parallel with NbO_2 layers with the magnetic field applied both out-of-plane and in-plane H. Superconductivity disappeared under the out-of-plane H at 0.9 T, whereas it remained robust under the in-plane H, indicating a large anisotropy of the upper critical field (H_{c2}). Figure 3(c) shows a contour image of ρ at 1.9 K mapped against H and the field angle (θ). The observed abrupt contrast indicates a single peak at 4.1 T and $\theta = 90°$ and slopes approaching 0.69 T when $\theta = 0°$ or $\theta = 180°$. The anisotropy of H_{c2} was thus evaluated six times, as discussed below.

For further analysis, we extracted 90% normal-state ρ to estimate H_{c2} following a previous study for bulk [24], and plotted them as a function of θ [Fig. 3(d)]. The inset shows the resistivity as a function of H for θ ranging from 0° to 90°. Then, the profile of $\mu_0 H_{c2}$ vs θ was analyzed based on the anisotropic Ginzburg-Landau (GL) theory and the 2D Tinkham model. For thre-dimensional (3D) systems, the GL

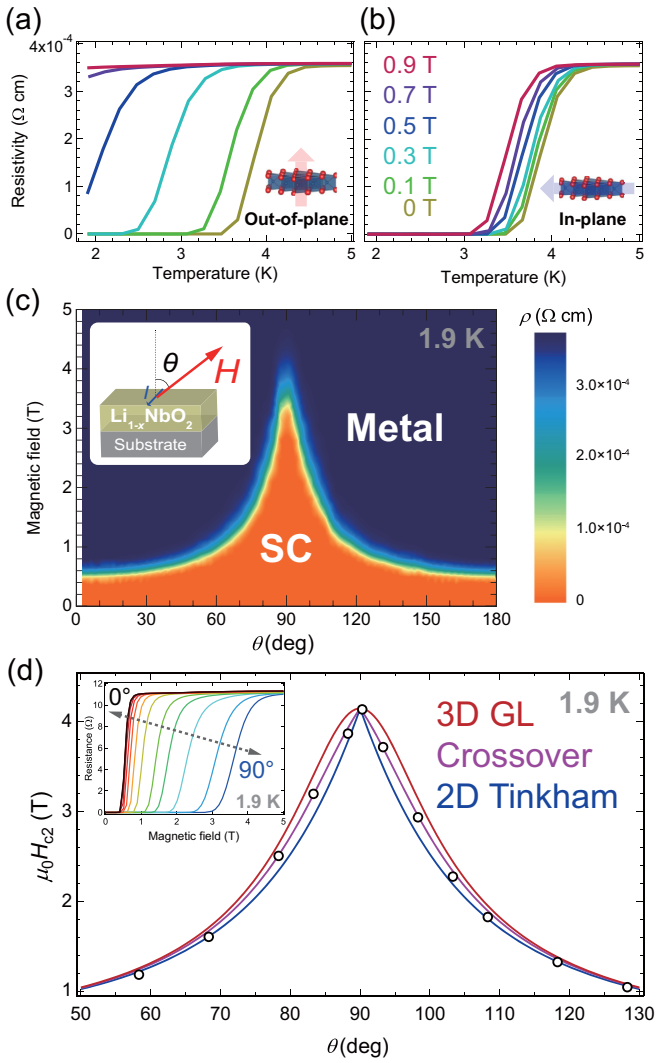

FIG. 3. Anisotropy of upper critical field for $Li_{1-x}NbO_2$ films (sample B). Magnetic-field (H) dependence of ρ-T curves with the applied field: (a) out of plane ($\theta = 0°$), and (b) in plane ($\theta = 90°$). (c) Contour image in color scale for ρ measured at 1.9 K for different H and angles. The measurement configuration of the sample, H, θ, and current (I) is shown in the inset. (d) $\mu_0 H_{c2}$ at 1.9 K as a function of the θ, with fits to 3D Ginzburg-Landau (red) and 2D Tinkham (blue) models, and their crossover (purple, $\alpha = 0.5$) derived by using Eqs. (1)–(3), respectively. The inset shows H dependence of ρ measured at various θ.

theory describes $H_{c2}(\theta)$ as [25,26]

$$\left[\frac{H_{c2}(\theta)\sin\theta}{H_{c2}^{\perp}}\right]^2+\left[\frac{H_{c2}(\theta)\cos\theta}{H_{c2}^{\parallel}}\right]^2=1, \tag{1}$$

where $H_{c2}^{\perp}$ and $H_{c2}^{\parallel}$ are H_{c2} along the out-of-plane ($\theta = 0°$) and in-plane ($\theta = 90°$) directions, respectively. By contrast, the Tinkham model is used for the 2D limit, where superconducting layers are considered to be ultimately isolated [25,26]. In this case, $H_{c2}(\theta)$ is given by

$$\left|\frac{H_{c2}(\theta)\sin\theta}{H_{c2}^{\perp}}\right|+\left[\frac{H_{c2}(\theta)\cos\theta}{H_{c2}^{\parallel}}\right]^2=1, \tag{2}$$

As shown in Fig. 3(d), Eqs. (1) and (2) give similar but notably different curves near $\theta = 90°$ and bracket the experimental data. This is common for crossovers between 2D and 3D systems. For such cases, Eqs. (1) and (2) can be combined as

$$\alpha\left|\frac{H_{c2}(\theta)\sin\theta}{H_{c2}^{\perp}}\right|+(1-\alpha)\left[\frac{H_{c2}(\theta)\sin\theta}{H_{c2}^{\perp}}\right]^2+\left[\frac{H_{c2}(\theta)\cos\theta}{H_{c2}^{\parallel}}\right]^2 = 1\ (0\leqslant\alpha\leqslant 1), \tag{3}$$

where α is a dimensionality parameter that reproduces Eqs. (1) and (2) when $\alpha = 0$ and 1, respectively [27–29]. Our data best fitted Eq. (3) with $\alpha = 0.5$, supporting a large anisotropy, even in thick and bulklike $Li_{1-x}NbO_2$ films. The ideal or nearly 2D superconductivity requires spatial carrier confinement, as also realized in artificial structures such as superlattices [27], atomic layer materials [11,12], $LaAlO_3/SrTiO_3$ interfaces [30], and field effect induced accumulation layers [31]. Moreover, naturally layered oxides such as cuprates and ruthenates exhibit 2D superconductivity with intrinsically large anisotropy [29,32]. The magnitude of the anisotropy can be quantitatively discussed based on the coherence length within the GL theory.

C. Ginzburg-Landau analysis for quantitative evaluations

For quantitative analyses of anisotropy, we measured the temperature dependence of magnetoresistance at $\theta = 0°$ and 90° [Figs. 4(a) and 4(b)] for sample B. We plotted $H_{c2}^{\parallel}$ and $H_{c2}^{\perp}$ as a function of temperature normalized by T_c (T/T_c) [Fig. 4(c)]. The two variables showed substantially different magnitudes but identical temperature dependences. In addition, they traced up and down along H_{c2} reported previously for polycrystalline bulk $Li_{1-x}NbO_2$ [24]. This result is remarkable because $H_{c2}^{\parallel}$ and $H_{c2}^{\perp}$ clearly determined here have never been distinguished in randomly oriented crystals. Both H_{c2} fitted the generalized GL equation shown as broken curves, $H_{c2}(T) = H_{c2}(0)[1-(T/T_c)^2)/[1+(T/T_c)^2]$ [25,26,33]. This is inconsistent with the square-root temperature dependence often observed for ideal 2D systems [27,33]. Therefore, it is concluded that $Li_{1-x}NbO_2$ is located in the region of the crossover from 2D to 3D. Note that similar trends are found in other dimensional crossover systems [27,29,33].

Having established $H_{c2}^{\parallel}$ and $H_{c2}^{\perp}$, the in-plane and out-of-plane coherence lengths can be evaluated as $\xi^{\parallel}(T) = \sqrt{\Phi_0/[2\pi H_{c2}^{\perp}(T)]}$ and $\xi^{\perp}(T) = \sqrt{\Phi_0 H_{c2}^{\perp}(T)/[2\pi H_{c2}^{\parallel}(T)^2]}$, respectively [26,33], where Φ_0 is the superconducting magnetic flux quantum. Using the aforementioned $H_{c2}^{\parallel}$ and $H_{c2}^{\perp}$, we obtained $\xi^{\parallel} = 22$ nm and $\xi^{\perp} = 3.7$ nm at 1.9 K. These values exhibit the above-described temperature dependence, and approached the constants (18 and 2.9 nm) at $T = 0$ K (Supplemental Material [19]). The $\xi^{\perp}$ of 3.7 nm exceeds the NbO_2 layer spacing (0.52 nm), but is comparable to $\xi^{\perp}$ of bulk TMDs [34]. As expected from the structural similarity (Fig. 1), $Li_{1-x}NbO_2$ and TMDs have similar dimensionality. The ratio of $\xi^{\parallel}$ to $\xi^{\perp}$ is known as the anisotropy ratio γ, which is equal to 6. By definition, γ is equal to $H_{c2}^{\parallel}/H_{c2}^{\perp}$. It is reasonable, therefore, to suggest that superconductivity in $Li_{1-x}NbO_2$ occurs at 2D NbO_2^- layers with Li^+-ion blocking layers that also act as a charge reservoir. In this regard, $Li_{1-x}NbO_2$ can

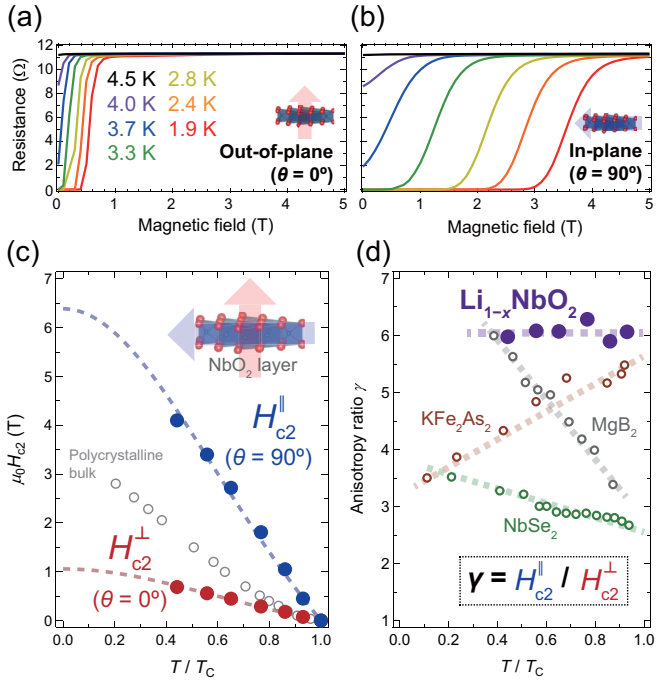

FIG. 4. Temperature dependencies of upper critical field and anisotropy (sample B). Magnetic-field dependence of resistance at different temperatures with the field applied: (a) out of plane ($\theta = 0°$) and (b) in plane ($\theta = 90°$). (c) $\mu_0 H_{c2}$ as a function of T/T_c. Red and blue filled circles indicate the out-of-plane and in-plane H_{c2}, respectively. The polycrystalline bulk data [24] are also shown with open circles. Broken curves indicate theoretical curves calculated with the generalized GL equation. (d) Anisotropy ratio ($\gamma = H_{c2}^{\parallel}/H_{c2}^{\perp}$) as a function of T/T_c. Purple filled circles indicate our data. The data for MgB_2 [36], KFe_2As_2 [39], and $NbSe_2$ [40,41] are also shown in gray, brown, and green open circles, respectively. Broken lines guide the eye.

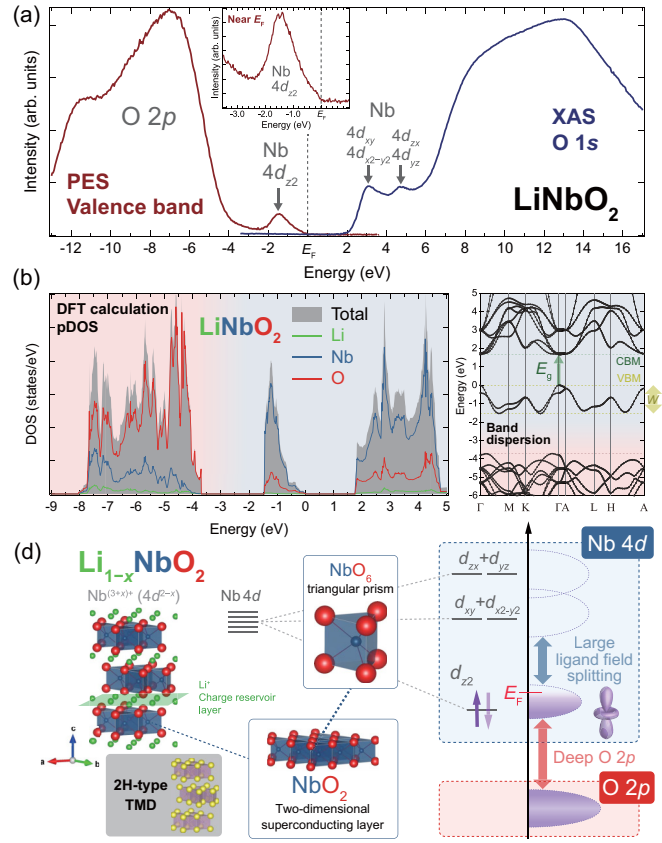

FIG. 5. Electronic structure of two-dimensional and single-band character of $Li_{1-x}NbO_2$. (a) Synchrotron-radiation PES and O 1*s* XAS for the $LiNbO_2$ film. The energy was scaled as a value relative to the E_F. Inset shows magnified PES near E_F. DFT calculations for $LiNbO_2$ showing (b) projected density of states, and (c) band dispersion. (d) Schematic illustrations of crystal structure and band diagram for $Li_{1-x}NbO_2$. The superconducting "2*H*-NbO_2" layers consist of edge-shared triangular prisms that exhibit large ligand field splitting of Nb 4*d* states. Strong ionicity of oxygen places the O 2*p* state far below E_F resulting in the correlated single-band character of the d_{z^2} state.

be classified into both classes of TMDs and layered cuprate superconductors. Interestingly, the $\xi^{\parallel}/\xi^{\perp}$ ratio for $Li_{1-x}NbO_2$ is comparable to those of a number of cuprates, including YBa_2Cu_3O [35]. Based on the GL theory, the effective mass ratio is deduced as $m^{*\perp}/m^{*\parallel} = \gamma^2 = 36$, also supporting large anisotropy in $Li_{1-x}NbO_2$.

We discovered a temperature-independent γ, which is remarkable because in most TMD-based and other superconductors γ varies significantly with temperature [Fig. 4(d)]. The temperature dependence of γ strongly reflects the electronic states near the Fermi level (E_F) and provides insight into multiband superconductors [36,37]. Conversely, the properties of single-band superconductors manifest themselves in a constant γ, where a single band solely governs superconductivity regardless of the temperature [38]. The previous results for multiband superconductors, MgB_2, KFe_2As_2, and 2*H*-$NbSe_2$, are also shown in Fig. 4(d) for comparison [36,39–41]. In addition to a temperature-dependent γ, multiband structures of 2*H*-$NbSe_2$ have been confirmed by angle-resolved PES [42,43]. The different electronic states arise from individual chemical bonding, highlighting the unique 2*H*-type oxide superconductor.

D. Strongly isolated single-band structure of 2*H*-NbO_2 layer

Synchrotron-radiation spectroscopic measurements revealed the unique electronic states associated with the NbO_2 layer. We used pristine $LiNbO_2$ films capped with ultrathin amorphous Al_2O_3 deposited *in situ* to prevent sample surface degradation [14]. Figure 5(a) shows the PES near the E_F and O 1*s* XAS. The XAS energy scale was shifted so that its preedge with respect to the valence band maximum matched the band gap determined by optical absorption measurements [14] for obtaining a "combined plot" representing overall electronic structure near E_F [44,45]. The broad density of states (DOS) between −13 and −4 eV is composed mainly of O 2*p* states, as is commonly observed for other metal oxides [46]. The narrow DOS just below E_F, magnified in the inset of Fig. 5(a), was mainly derived from the Nb 4*d* states. No DOS was observed at E_F, indicating the insulating ground state of stoichiometric $LiNbO_2$ [14,47]. The XAS for the O 1*s* state provides the DOS for empty states derived from the large hybridization of O 2*p* to Nb 4*d* states [48], revealing

two prominent features at 3.1 and 4.8 eV that are also derived from the Nb 4*d* states. A total of three peaks is primarily due to ligand field splitting in the Nb 4*d* states, and are weighted with d_{z2}, $d_{xy} + d_{x2\text{-}y2}$, and $d_{zx} + d_{yz}$, respectively [2–8].

Comparison of the PES and XAS spectra to DFT-calculated projected DOS (pDOS) [Fig. 5(b)] shows good agreement. Three peaks were reproduced by the pDOS near E_F, where the Nb 4*d* states were predominant with O 2*p* hybridization and the remaining 4*d* states overlapped with deep O 2*p* states. The band dispersion also indicated largely isolated Nb 4*d* states [Fig. 5(c)]. The bandwidth W for the Nb $4d_{z2}$ states was ∼1.5 eV, much narrower than for perovskite-type niobates with octahedral lattices [46]. When holes are doped into the Nb $4d_{z2}$ band by Li deficiency, superconductivity occurs in $Li_{1\text{-}x}NbO_2$. Thus, 2D carriers confined in the narrow single band play an important role in the correlated electronic properties of 2*H*-NbO_2.

IV. DISCUSSION

The clear evidence of the 2D and single-band characteristics of superconductivity with isolated Nb $4d_{z2}$ states enables the following description of the electronic states of 2*H*-NbO_2. As shown in Fig. 5(d), the unique band structure originates from structural similarity to TMDs and the strong ligand field. The electronegativity of ligand atoms affects ligand field splitting and the energetic isolation of transition-metal *d* states from ligand atom *p* states. The fundamental band gap (E_g) of $LiNbO_2$ is as wide as ∼2 eV, and increases to ∼2.4 eV with hole doping [14]. Moreover, the fact that E_g exhibits the minimum at the Γ point is intriguing for possible optical functionality. By contrast, TMDs show a much narrower E_g, e.g., only 1.2 eV (indirect) for 2*H*-MoS_2 [9]. For $NbSe_2$, the Fermi surface consists of strongly hybridized Nb 4*d* and Se 4*p* states [42,43]. The unique electronic states of $Li_{1\text{-}x}NbO_2$ lead to high optical transparency despite the presence of high-density hole carriers [14].

Our study sheds light on exotic superconductors within the framework of single-band Hubbard systems [49]. Due to the layered structures and giant Jahn-Teller splitting, most high-T_c cuprates exhibit 2D characteristics, with a single $3d_{x2\text{-}y2}$ band with W smaller than the on-site Coulomb repulsion U [50]. The search for other classes of superconducting materials involving 2D and single-band characters has been a long-standing challenge, also motivating recent materials informatics efforts [50,51]. Sr_2IrO_4 is considered a good candidate due to the correlated 2D properties of the IrO_2 layer with a single band realized by strong spin-orbit coupling [52]. In addition, it has long been discussed that quantum fluctuations arising from geometrically frustrated 2D triangular lattices are favorable for strongly correlated superconductivity [53,54], as investigated in LiV_2O_4 and layered $Na_xCoO_2 \cdot yH_2O$ [55,56].

The electronic properties of $Li_{1\text{-}x}NbO_2$ can also be understood as a doped Mott insulator. Lee *et al.* predicted that the Li-free pristine 2*H*-NbO_2 is a half-filled Mott-Hubbard insulator with a 2D triangular lattice, single Nb $4d_{z2}$ band, narrow W, and strong U [47]. Recently, the ideal 2D triangular-lattice Hubbard system has been verified experimentally for TMD moiré superlattices [17,18]. This guides us to further investigate $Li_{1\text{-}x}NbO_2$ exhibiting a heavy mass of hole carriers and a crossover between Fermi liquid and non-Fermi-liquid behaviors ($\rho \propto T^2$ vs $\rho \propto T$) [14], implying 2D antiferromagnetic fluctuations [57]. Therefore, 2*H*-NbO_2 can be an ideal platform for understanding the correlated electronic properties of 2D triangular-lattice Hubbard systems.

V. CONCLUSION

In summary, we have investigated the electronic states of 2*H*-NbO_2 layers as an ionic analog of van der Waals materials. The observation of a clear BKT transition and largely anisotropic H_{c2} in $Li_{1\text{-}x}NbO_2$ epitaxial films reveals that superconductivity occurs in the 2D to 3D crossover. The angle dependence of H_{c2} is reproduced by averaging the 3D and 2D models' contributions. According to the GL theory, the superconducting coherence lengths parallel and perpendicular to the NbO_2 layer approach 18 and 2.9 nm, respectively, at $T = 0$ K. These properties are similar to those of TMDs and cuprates. On the other hand, single-band superconductivity is strongly suggested by the temperature-independent anisotropy ratio, synchrotron-radiation PES measurements, and DFT calculations. The superconductivity at a correlated narrow band is also reminiscent of cuprates, but differs from TMDs. We conclude that the nature of ionic bonding and the triangular prism coordination lead to a narrow Nb 4*d* band at E_F that is largely isolated from the O 2*p* states. Such electronic states favor the accommodation of correlated electrons with the triangular-lattice Hubbard system.

ACKNOWLEDGMENTS

The authors thank Honorary Professor Hideo Hosono and Professor Hidenori Hiramatsu for their support with angle-dependent magnetotransport measurements. This work was partly supported by the MEXT Elements Strategy Initiative to the Form Core Research Center (Grant No. JPMXP0112101001), JSPS KAKENHI (Grants No. 19H02588, No. 20K15169, and No. 21H02026), and the Yoshinori Ohsumi Fund for Fundamental Research. The work at KEK-PF was conducted with the approval of the Program Advisory Committee (Proposals No. 2017G596, No. 2018S2-004, No. 2019G583, No. 2021G660, and No. 2021G683) at the Institute of Materials Structure Science, KEK, Japan.

[1] M. J. Gaselbracht, T. J. Richardson, and A. M. Stacy, Superconductivity in the layered compound Li_xNbO_2, Nature (London) **345**, 324 (1990).

[2] A. Miura, K. Tadanaga, E. Magome, C. Moriyoshi, Y. Kuroiwa, T. Takahiro, and N. Kumada, Octahedral and trigonal-prismatic coordination preferences in Nb-, Mo-, Ta-, and W-based ABX_2

layered oxides, oxynitrides, and nitrides, J. Solid State Chem. **229**, 272 (2015).

[3] D. Waroquiers, X. Gonze, G.-M. Rignanese, C. Welker-Nieuwoudt, F. Rosowski, M. Göbel, S. Schenk, P. Degelmann, R. André, R. Glaum, and G. Hautier, Statistical analysis of coordination environments in oxides, Chem. Mater. **29**, 8346 (2017).

[4] R. A. D. Wentworth, Trigonal prismatic vs. octahedral stereochemistry in complexes derived from innocent ligands, Coord. Chem. Rev. **9**, 171 (1972).

[5] E. Cremades, J. Echeverría, and S. Alvarez, The trigonal prism in coordination chemistry, Chem. Eur. J. **16**, 10380 (2010).

[6] M. Kertesz and R. Hoffmann, Octahedral vs. trigonal-prismatic coordination and clustering in transition-metal dichalcogenides, J. Am. Chem. Soc. **106**, 3453 (1984).

[7] M. Chhowalla, H. S. Shin, G. Eda, L.-J. Li, K. P. Loh, and H. Zhang, The chemistry of two-dimensional layered transition metal dichalcogenide nanosheets, Nat. Chem. **5**, 263 (2013).

[8] H. Yang, S. W. Kim, M. Chhowalla, and Y. H. Lee, Structural and quantum-state phase transitions in van der Waals layered materials, Nat. Phys. **13**, 931 (2017).

[9] Q. H. Wang, K. Kalantar-Zadeh, A. Kis, J. N. Coleman, and M. S. Strano, Electronics and optoelectronics of two-dimensional transition metal dichalcogenides, Nat. Nanotechnol. **7**, 699 (2012).

[10] X. Xu, W. Yao, D. Xiao, and T. F. Heinz, Spin and pseudospins in layered transition metal dichalcogenides, Nat. Phys. **10**, 343 (2014).

[11] J. M. Lu, O. Zheliuk, I. Leermakers, N. F. Q. Yuan, U. Zeitler, K. T. Law, and J. T. Ye, Evidence for two-dimensional Ising superconductivity in gated MoS_2, Science **350**, 1353 (2015).

[12] X. Xi, Z. Wang, W. Zhao, J.-H. Park, K. T. Law, H. Berger, L. Forró, J. Shan, and K. F. Mak, Ising pairing in superconducting $NbSe_2$ atomic layers, Nat. Phys. **12**, 139 (2016).

[13] A. Devarakonda, H. Inoue, S. Fang, C. Ozsoy-Keskinbora, T. Suzuki, M. Kriener, L. Fu, E. Kaxiras, D. C. Bell, and J. G. Checkelsky, Evidence for clean 2D superconductivity and field-induced finite-momentum pairing in a bulk vdW superlattice, Science **370**, 231 (2020).

[14] T. Soma, K. Yoshimatsu, and A. Ohtomo, *p*-Type transparent superconductivity in a layered oxide, Sci. Adv. **6**, eabb8570 (2020).

[15] L. Zhang, Y. Zhou, L. Guo, W. Zhao, A. Barnes, H.-T. Zhang, C. Eaton, Y. Zheng, M. Brahlek, H. F. Haneef, N. J. Podraza, M. H. W. Chan, V. Gopalan, K. M. Rabe, and R. Engel-Herbert, Correlated metals as transparent conductors, Nat. Mater. **15**, 204 (2016).

[16] W. S. Yun, S. W. Han, S. C. Hong, I. G. Kim, and J. D. Lee, Thickness and strain effects on electronic structures of transition metal dichalcogenides: 2H-MX_2 semiconductors (M = Mo, W; X = S, Se, Te), Phys. Rev. B **85**, 033305 (2012).

[17] F. Wu, T. Lovorn, E. Tutuc, A. H. MacDonald, and A. H. Hubbard, Model Physics in Transition Metal Dichalcogenide Moiré Bands, Phys. Rev. Lett. **121**, 026402 (2018).

[18] Y. Tang, L. Li, T. Li, Y. Xu, S. Liu, K. Barmak, K. Watanabe, T. Taniguchi, A. H. MacDonald, J. Shan, and K. F. Mak, Simulation of Hubbard model physics in WSe_2/WS_2 moiré superlattices, Nature (London) **579**, 353 (2020).

[19] See Supplemental Material at http://link.aps.org/supplemental/10.1103/PhysRevB.105.104504 for calculation details, sample information, and supporting analysis.

[20] P. Giannozzi, S. Baroni, N. Bonini, M. Calandra, R. Car, C. Cavazzoni, D. Ceresoli, G. L. Chiarotti, M. Cococcioni, I. Dabo, A. D. Corso, S. de Gironcoli, S. Fabris, G. Fratesi, R. Gebauer, U. Gerstmann, C. Gougoussis, A. Kokalj, M. Lazzeri, L. Martin-Samos *et al.*, QUANTUM ESPRESSO: A modular and open-source software project for quantum simulations of materials, J. Phys.: Condens. Matter **21**, 395502 (2009).

[21] P. Giannozzi, O. Andreussi, T. Brumme, O. Bunau, M. B. Nardelli, M. Calandra, R. Car., C. Cavazzoni, D. Ceresoli, M. Cococcioni, N. Colonna, I. Carnimeo, A. D. Corso, S. de Gironcoli, P. Delugas, R. A. DiStasio, Jr., A. Ferretti, A. Floris, G. Fratesi, G. Fugallo *et al.*, Advanced capabilities for materials modelling with QUANTUM ESPRESSO, J. Phys.: Condens. Matter **29**, 465901 (2017).

[22] M. R. Beasley, J. E. Mooij, and T. P. Orlando, Possibility of Vortex-Antivortex Pair Dissociation in Two-Dimensional Superconductors, Phys. Rev. Lett. **42**, 1165 (1979).

[23] B. I. Halperin and D. R. Nelson, Resistive transition in superconducting films, J. Low Temp. Phys. **36**, 599 (1979).

[24] G. T. Liu, J. L. Luo, Z. Li, Y. Q. Guo, N. L. Wang, and D. Jin, Evidence of *s*-wave pairing symmetry in the layered superconductor $Li_{0.68}NbO_2$ from specific heat measurements, Phys. Rev. B **74**, 012504 (2006).

[25] M. Tinkham, Effect of fluxoid quantization on transitions of superconducting films, Phys. Rev. **129**, 2413 (1963).

[26] M. Tinkham, *Introduction to Superconductivity*, 2nd ed. (Dover Publications, New York, 2004).

[27] S. T. Ruggiero, T. W. Barbee, Jr., and M. R. Beasley, Superconductivity in Quasi-Two-Dimensional Layered Composites, Phys. Rev. Lett. **45**, 1299 (1980).

[28] S. K. Goh, Y. Mizukami, H. Shishido, D. Watanabe, S. Yasumoto, M. Shimozawa, M. Yamashita, T. Terashima, Y. Yanase, T. Shibauchi, A. I. Buzdin, and Y. Matsuda, Anomalous Upper Critical Field in $CeCoIn_5/YbCoIn_5$ Superlattices with a Rashba-Type Heavy Fermion Interface, Phys. Rev. Lett. **109**, 157006 (2012).

[29] M. Uchida, M. Ide, M. Kawamura, K. S. Takahashi, Y. Kozuka, Y. Tokura, and M. Kawasaki, Anomalous enhancement of upper critical field in Sr_2RuO_4 thin films, Phys. Rev. B **99**, 161111(R) (2019).

[30] A. M. R. V. L. Monteiro, D. J. Groenendijk, I. Groen, J. de Bruijckere, R. Gaudenzi, H. S. J. van der Zant, and A. D. Caviglia, Two-dimensional superconductivity at the (111) $LaAlO_3/SrTiO_3$ interface, Phys. Rev. B **96**, 020504(R) (2017).

[31] K. Ueno, T. Nojima, S. Yonezawa, M. Kawasaki, Y. Iwasa, and Y. Maeno, Effective thickness of two-dimensional superconductivity in a tunable triangular quantum well of $SrTiO_3$, Phys. Rev. B **89**, 020508(R) (2014).

[32] R. Fastampa, M. Giura, R. Marcon, and E. Silva, 2D to 3D crossover in Bi-Sr-Ca-Cu-O: Comparison with Synthetic Multilayered Superconductors, Phys. Rev. Lett. **67**, 1795 (1991).

[33] Q. R. Zhang, D. Rhodes, B. Zeng, M. D. Johannes, and L. Balicas, Non-Ising-like two-dimensional superconductivity in a bulk single crystal, Phys. Rev. B **94**, 094511 (2016).

[34] J. A. Woollam and R. B. Somoano, Superconducting critical fields of alkali and alkaline-earth intercalates of MoS_2, Phys. Rev. B **13**, 3843 (1976).

[35] V. S. Zapf, N.-C. Yeh, A. D. Beyer, C. R. Hughes, C. H. Mielke, N. Harrison, M. S. Park, K. H. Kim, and S.-I. Lee, Dimensionality of superconductivity and vortex dynamics in the infinite-layer cuprate $Sr_{0.9}M_{0.1}CuO_2$ (M = La, Gd), Phys. Rev. B **71**, 134526 (2005).

[36] M. Angst, R. Puzniak, A. Wisniewski, J. Jun, S. M. Kazakov, J. Karpinski, J. Roos, and H. Keller, Temperature and Field Dependence of the Anisotropy of MgB_2, Phys. Rev. Lett. **88**, 167004 (2002).

[37] F. Hunte, J. Jaroszynski, A. Gurevich, D. C. Larbalestier, R. Jin, A. S. Sefat, M. A. McGuire, B. C. Sales, D. K. Christen, and D. Mandrus, Two-band superconductivity in $LaFeAsO_{0.89}F_{0.11}$ at very high magnetic fields, Nature (London) **453**, 903 (2008).

[38] A. A. Golubov and A. E. Koshelev, Upper critical field in dirty two-band superconductors: Breakdown of the anisotropic Ginzburg-Landau theory, Phys. Rev. B **68**, 104503 (2003).

[39] T. Terashima, M. Kimata, H. Satsukawa, A. Harada, K. Hazama, S. Uji, H. Harima, G.-F. Chen, J.-L. Luo, and N.-L. Wang, Resistivity and upper critical field in KFe_2As_2 single crystals, J. Phys. Soc. Jpn. **78**, 063702 (2009).

[40] N. Toyota, J. Nakatsuji, K. Noto, A. Hoshi, N. Kobayashi, Y. Muto, and Y. Onodera, Temperature and angular dependences of upper critical fields for the layer structure superconductor $2H$-$NbSe_2$, J. Low Temp. Phys. **25**, 485 (1976).

[41] L. Chen, J. Zuo, Y. Lu, and H. Huang, Two-band calculations on the upper critical field of superconductor $NbSe_2$, Physica C (Amsterdam, Neth.) **471**, 1591 (2011).

[42] T. Yokoya, T. Kiss, A. Chainani, S. Shin, M. Nohara, and H. Takagi, Fermi surface sheet dependent superconductivity in $2H$-$NbSe_2$, Science **294**, 2518 (2001).

[43] Y. Noat, J. A. Silva-Guillén, T. Cren, V. Cherkez, C. Brun, S. Pons, F. Debontridder, D. Roditchev, W. Sacks, L. Cario, P. Ordejón, A. García, and E. Canadell, Quasiparticle spectra of $2H$-$NbSe_2$: Two-band superconductivity and the role of tunneling selectivity, Phys. Rev. B **92**, 134510 (2015).

[44] M. Takizawa, D. Toyota, H. Wadati, A. Chikamatsu, H. Kumigashira, A. Fujimori, M. Oshima, Z. Fang, M. Lippmaa, M. Kawasaki, and H. Koinuma, Manifestation of correlation effects in the photoemission spectra of $Ca_{1-x}Sr_xRuO_3$, Phys. Rev. B **72**, 060404(R) (2005).

[45] K. H. L. Zhang, Y. Du, A. Papadogianni, O. Bierwagen, S. Sallis, L. F. J. Piper, M. E. Bowden, V. Shutthanandan, P. V. Sushko, and S. A. Chambers, Perovskite Sr-doped $LaCrO_3$ as a new p-type transparent conducting oxide, Adv. Mater. **27**, 5191 (2015).

[46] Y. Park, J. Roth, D. Oka, Y. Hirose, T. Hasegawa, A. Paul, A. Pogrebnyakov, V. Gopalan, T. Birol, and R. Engel-Herbert, $SrNbO_3$ as a transparent conductor in the visible and ultraviolet spectra, Commun. Phys. **3**, 102 (2020).

[47] K.-W. Lee, J. Kuneš, R. T. Scalettar, and W. E. Pickett, Correlation effects in the triangular lattice single-band system Li_xNbO_2, Phys. Rev. B **76**, 144513 (2007).

[48] H.-J. Noh, B. J. Kim, S.-J. Oh, J.-H. Park, H.-J. Lin, C. T. Chen, Y. S. Lee, K. Yamaura, and E. Takayama-Muromachi, Comparative study of the electronic structures of $SrMO_3$ (M = Ti, V, Mn, Fe, and Co; M = Zr, Mo, Ru, and Rh) by O 1s x-ray absorption spectroscopy, J. Phys.: Condens. Matter **20**, 485208 (2008).

[49] J. Hubbard, Electron correlations in narrow energy bands, Proc. R. Soc. London, Ser. A **276**, 238 (1963).

[50] E. B. Isaacs and C. Wolverton, Materials Informatics Approach to the Identification of One-Band Correlated Materials Analogous to the Cuprates, Phys. Rev. X **9**, 021042 (2019).

[51] S. M. Griffin, P. Staar, T. C. Schulthess, M. Troyer, and N. A. Spaldin, A bespoke single-band Hubbard model material, Phys. Rev. B **93**, 075115 (2016).

[52] B. J. Kim, H. Jin, S. J. Moon, J.-Y. Kim, B.-G. Park, C. S. Leem, J. Yu, T. W. Noh, C. Kim, S.-J. Oh, J.-H. Park, V. Durairaj, G. Cao, and E. Rotenberg, Novel $J_{\rm eff} = 1/2$ Mott State Induced by Relativistic Spin-Orbit Coupling in Sr_2IrO_4, Phys. Rev. Lett. **101**, 076402 (2008).

[53] S. Burdin, D. R. Grempel, and A. Georges, Heavy-fermion and spin-liquid behavior in a Kondo lattice with magnetic frustration, Phys. Rev. B **66**, 045111 (2002).

[54] K. S. Chen, Z. Y. Meng, U. Yu, S. Yang, M. Jarrell, and J. Moreno, Unconventional superconductivity on the triangular lattice Hubbard model, Phys. Rev. B **88**, 041103(R) (2013).

[55] N. E. Hussey, Non-generality of the Kadowaki–Woods ratio in correlated oxides, J. Phys. Soc. Jpn. **74**, 1107 (2005).

[56] T. Fujimoto, G.-q. Zheng, Y. Kitaoka, R. L. Meng, J. Cmaidalka, and C. W. Chu, Unconventional Superconductivity and Electron Correlations in the Cobalt Oxyhydrate $Na_{0.35}CoO_2 \cdot yH_2O$ from Nuclear Quadrupole Resonance, Phys. Rev. Lett. **92**, 047004 (2004).

[57] G. R. Stewart, Non-Fermi-liquid behavior in d- and f-electron metals, Rev. Mod. Phys. **73**, 797 (2001).